






Requirements on quantum superpositions of macro-objects for sensing neutrinos

Eva Kilian ^{1,*} Marko Toroš ² Frank F. Deppisch ¹ Ruben Saakyan ¹ and Sougato Bose ¹

¹*Department of Physics & Astronomy, University College London, WC1E 6BT London, United Kingdom*

²*School of Physics & Astronomy, University of Glasgow, Glasgow, G12 8QQ, United Kingdom*



(Received 25 May 2022; accepted 22 January 2023; published 7 April 2023)

We examine a macroscopic system in a quantum superposition of two spatially separated localized states as a detector for a stream of weakly interacting relativistic particles. We do this using the explicit example of neutrinos with MeV-scale energy scattering from a solid object via neutral-current neutrino-nucleus scattering. Presuming the (anti)neutrino source to be a nuclear fission reactor, we utilize the estimated flux and coherent elastic neutrino-nucleus cross section to constrain the spatial separation Δx and describe the temporal evolution of the sensing system. Particularly, we find that a potentially measurable relative phase between quantum superposed components is obtained for a single gram scale mass placed in a superposition of spatial components separated by 10^{-14} m under sufficient cooling and background suppression.

DOI: [10.1103/PhysRevResearch.5.023012](https://doi.org/10.1103/PhysRevResearch.5.023012)

I. INTRODUCTION

Despite extensive scientific efforts, neutrinos still pose a puzzling enigma, decades after they were first observed experimentally [1]. While it may be known that neutrinos interact only through the weak and the gravitational forces, many of the questions on the very nature of these particles remain unanswered to this day. As all other fermions in the standard model, neutrinos were formerly assumed to be representable by Dirac spinors and additionally thought to be massless. However, oscillation experiments have shown that particles produced in a particular, well-defined flavor eigenstate can, after having traveled a sufficiently long distance, with a certain probability be detected in a different flavor state [2]. A consequence of these findings is that neutrinos do have mass and that their flavor eigenstates are different from their mass eigenstates. As a result of being massive, neutrinos could be either Dirac or Majorana particles and it is currently unknown which of the two they are. Present-day oscillation experiments enable measurements of mass-squared differences of the three neutrino mass eigenstates, but they are not capable of measuring absolute neutrino masses, on which limits however exist [3]. In addition, oscillation experiments have also seen hints for the existence of so-called sterile neutrinos. These are hypothetical additional species of neutrinos that do not experience any of the standard model forces but would mix with the three standard neutrinos. The vast multitude of unknowns provides a motivation to seek novel methods to detect neutrinos, especially to examine if the detector size can be

reduced. In this work, we will introduce one such approach aiming to study reactor antineutrinos with energies of a few MeV through their *momentum transfer* in scattering from a macroscopic system placed in a quantum superposition of distinct center of mass positions—with the momentum transfer appearing as a relative phase between the components of the superposition.

The field of matter-wave interferometry in which a large mass, such as a solid object or crystal of several atoms, goes to a quantum superposition of being “here” and “there” is an emerging area still in development, with several nascent ideas. For an inexhaustive list see Refs. [4–16]. These developments have so far been primarily steered by the aim to extend the boundaries of quantum mechanics *empirically* to larger objects, as the quantum behavior of the center of mass (COM) of a sufficiently macroscopic masses remains untested. Unlike in the case of interference experiments with several atoms from a cold source, for example a Bose-Einstein condensate, where each atom goes one way or another, here *all* atoms of the crystal go one way together or *all* atoms of the crystal go the other way together. On the experimental side these developments are stimulated, on the one hand, by the demonstration of quantum superpositions of the COM of large molecules consisting of up to ~ 2000 atoms [17] and, on the other hand, by the achievement of cooling of the COM of much larger masses such as 10^{-17} kg nanocrystals [18–21] and 10 kg masses [22] close to their quantum mechanical ground states. While this may still indicate a significant gap between what has been demonstrated, and what needs to be achieved to realize experiments with the COM of large masses in a superposition, there are the above well formulated schemes and conditions which could be adapted.

Quantum superpositions of the COM of large masses can have a great potential as a sensor [23]. It has already been theoretically demonstrated that they can measure tiny gravitational effects including the detection of low frequency gravitational waves [24], and, ultimately, even evidence the

*eva.kilian.18@ucl.ac.uk

quantum nature of gravity [25–28] or be able to test new forces [29] and the weak Equivalence principle in a quantum regime [30]. The decoherence of quantum superpositions may also be a sensitive detector for dark matter [31–33]. Once a quantum superposition of a large mass being in two positions is produced, external forces cause a relative phase shift between the two components of this superposition. Hence, we propose that it might also be possible to detect tiny momentum transfers due to the scattering of weakly interacting particles from such superpositions. In particular, recently the approach of detecting particles beyond the standard model via the momentum recoil of several levitated nano-objects in localized (classical) states has become topical [34,35]. It is natural thus to ask whether quantum superpositions can aid further. We study this herewith using neutrinos as an example, importantly in a regime in which they scatter coherently from entire nuclei as that significantly enhances the cross section.

Predicted more than 40 years ago in 1974 [36] and recently observed experimentally [37], coherent elastic scattering of neutrinos from nuclei (CE ν NS) is the dominant scattering channel for incoming neutrino energies $E_\nu \ll 100$ MeV. The scattering coherence manifests in an enhancement of the cross-section, which scales with N^2 , with N being the number of neutrons in the nucleus. Up until recently, it has however been of great difficulty to detect such neutral current events, in part due to the large detector volumes (enough nuclei) and low energy thresholds required to detect the keV to sub-keV recoils of the nuclei.

In light of the advent of proposals for small-scale neutrino detectors [38,39] that aim to exploit the small recoil energies and relatively large CE ν NS cross section associated with scattering events in the (sub-)MeV neutrino energy regime, we consider the suitability of matter-wave interferometric schemes for detecting such processes. We emphasize that in contrast to classical methods, our approach is based on the detection of neutrinos via massive quantum devices and hence exploits features which are inherently quantum.

II. DETECTING PARTICULATE MATTER BY MEASURING A PHASE

The essence of the type of detector that we are considering here is given in Fig. 1. A mass is prepared in a quantum superposition of spatially distinct states. An ideal way to generate such a spatial superposition is by employing a Stern-Gerlach-type interferometric scheme with a single spin embedded in a mass. An archetypal example is the nitrogen-vacancy (NV) point defect in a diamond crystal, which carries a spin-1 (made of two electrons) [40]. However, any other point defect with an electronic spin in any other crystal [41] or a single dopant atom with an unpaired electronic spin implanted in a solid, as for example, used in certain designs of solid state quantum computers [42] will serve our purpose. It is understood that the atom carrying this spin is tightly bound to the rest of the crystal. Also we have to ensure that there is this single spin which can couple to external magnetic fields strongly (i.e., with the strength of a Bohr magneton) while there may be unpaired nuclear spins on various atoms in the crystal which couple with the much lower strength of nuclear magneton. While detailed studies can be found in Refs. [10–16,43], here

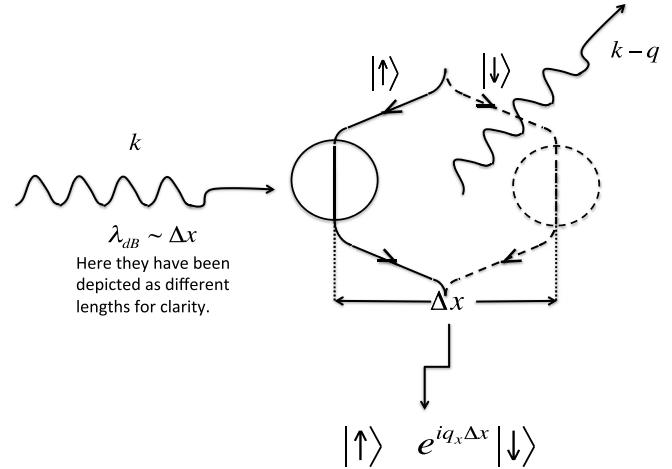


FIG. 1. The working mechanism of a system detecting the momentum recoil of a crystal due to the scattering of a particle from it through a phase between two components of a superposition. In a general Stern-Gerlach interferometer, the phase difference between two spatially separated components ends up as a phase difference between two spin states and can be measured as a phase difference between spin components.

we present only a schematic description. The spin is initially prepared in a quantum superposition $\frac{1}{\sqrt{2}}(|\uparrow\rangle_s + |\downarrow\rangle_s)$ and the mass bearing the spin is subjected to an inhomogeneous magnetic field. This couples its spin and motional degrees of freedom: for $|\uparrow\rangle_s$ spin state, the mass accelerates to the left, and for the $|\downarrow\rangle_s$ spin state, the mass accelerates to the right. They can be brought to a halt at a given superposition size Δx by flipping the spins at appropriate times. The resulting entangled state between spin and center of mass degree of freedom of the mass thus generated is

$$|\Psi_0\rangle_S = \frac{1}{\sqrt{2}}(|\uparrow\rangle_s |\bar{x}_0\rangle_C + |\downarrow\rangle_s |\bar{x}_1\rangle_C), \quad (1)$$

where $|\bar{x}_0\rangle_C$ and $|\bar{x}_1\rangle_C$, respectively, refer to both parts of the superposition, each one describing the center-of-mass motion of our test mass (crystal), while the subscript S denotes the combined system of spin and crystal. The states $|\bar{x}_j\rangle$ are to be understood as Gaussian wave packets localized around the position $(\bar{x}_j, 0, 0)$, and momentum $p \approx 0$. The superposition size is $\Delta x = \bar{x}_1 - \bar{x}_0$. For simple notation, we treat the macroscopic mass as a single particle and write the COM state of the macroscopic mass as

$$|\bar{x}_j\rangle_C = \left(\frac{1}{\sigma_c \sqrt{2\pi}} \right)^{\frac{1}{2}} \int_{-\infty}^{\infty} dx e^{-\frac{(x-\bar{x}_j)^2}{2\sigma_c^2}} \Psi_C^\dagger(x) |0\rangle, \quad (2)$$

where $\Psi_C^\dagger(x)$ creates the whole crystal at position $(x, 0, 0)$ and $|0\rangle$ is the vacuum state. Fundamentally, $|\bar{x}_j\rangle$ is a many-particle state. Hence, $\Psi_C^\dagger(x)$ is equal to a product of proton, neutron and electron creation operators at positions locked to, and distributed around, the COM position $(x, 0, 0)$.

Let us now find out what happens to the above Gaussian state $|\bar{x}_j\rangle$ when a momentum q is transferred to it. To model this, we assume momentum creation and annihilation operators of the mass to be b_k^\dagger and b_k , respectively, and study the

action on the state,

$$\begin{aligned}
 & \left(\int d^3\mathbf{k} b_{\mathbf{k}+\mathbf{q}}^\dagger b_{\mathbf{k}} \right) \int_{-\infty}^{\infty} dx e^{-\frac{(x-\bar{x}_j)^2}{2\sigma_c^2}} \Psi^\dagger(x)|0\rangle \\
 & \propto \int_{-\infty}^{\infty} dx e^{-\frac{(x-\bar{x}_j)^2}{2\sigma_c^2}} \int d^3\mathbf{k} b_{\mathbf{k}+\mathbf{q}}^\dagger b_{\mathbf{k}} \int d^3\mathbf{k}' e^{i\mathbf{k}'x} b_{\mathbf{k}'}^\dagger |0\rangle \\
 & = \int_{-\infty}^{\infty} dx e^{-\frac{(x-\bar{x}_j)^2}{2\sigma_c^2}} e^{-iq_x x} \int d^3(\mathbf{k}+\mathbf{q}) e^{i(\mathbf{k}+\mathbf{q})x} b_{\mathbf{k}+\mathbf{q}}^\dagger |0\rangle \\
 & = \int_{-\infty}^{\infty} dx e^{-\frac{(x-\bar{x}_j)^2}{2\sigma_c^2}} e^{-iq_x x} \Psi^\dagger(x)|0\rangle \\
 & = e^{-iq_x \bar{x}_j} e^{-\frac{q_x^2 \sigma_c^2}{2}} \int_{-\infty}^{\infty} dx e^{-\frac{(x-\bar{x}_j+iq_x \sigma_c^2)^2}{2\sigma_c^2}} \Psi^\dagger(x)|0\rangle. \quad (3)
 \end{aligned}$$

Considering the special case when the width of the Gaussian wave packet is much smaller than the length scale of the transferred momentum $\sigma_c \lesssim 1/q_x$, the state of the Gaussian after the momentum transfer is

$$e^{-iq_x \bar{x}_j} \int_{-\infty}^{\infty} dx e^{-\frac{(x-\bar{x}_j)^2}{2\sigma_c^2}} \Psi^\dagger(x)|0\rangle = e^{-iq_x \bar{x}_j} |\bar{x}_j\rangle, \quad (4)$$

implying that the initial state of a superposed mass and a scattering particle evolves as

$$|\Psi_0\rangle_S |\mathbf{p}\rangle_B \rightarrow |\Psi_{q_x}\rangle_S |\mathbf{p}-\mathbf{q}\rangle_B, \quad (5)$$

where we have introduced the label B to denote the bath environment composed of the scattering particle(s) and the subscript S to refer to the superposed target mass. The state $|\Psi_{q_x}\rangle_S$ is given by

$$|\Psi_{q_x}\rangle_S = \frac{1}{\sqrt{2}} (|\uparrow\rangle_{|\bar{x}_0}\rangle + e^{-iq_x \Delta x} |\downarrow\rangle_{|\bar{x}_1}\rangle), \quad (6)$$

where the difference in center-of-mass position is $\Delta x = \bar{x}_1 - \bar{x}_0$. A particle scattering from the above state and transferring a momentum \mathbf{q} to it, could be detected as a phase difference of $\frac{q_x \Delta x}{\hbar}$ (restoring the \hbar) between the components of the superposition, where q_x is the x -component of the momentum transfer. While a transfer of momentum with negligible transverse contributions represents an idealized scenario, it should be implicitly clear that in a more general scenario, we would have to consider the three-dimensional nature of the problem. In a typical Stern-Gerlach interferometry experiment, the two components $|\bar{x}_0\rangle$ and $|\bar{x}_1\rangle$ are brought back to completely overlap with each other by reversing the process which created them, as shown in Fig. 1 so that the spin state becomes $|\psi_{q_x}\rangle_s = \frac{1}{\sqrt{2}} (|\uparrow\rangle_s + e^{-iq_x \Delta x} |\downarrow\rangle_s)$. Thus, the phase is measurable purely from the off-diagonal component $\langle \uparrow | \rho_s | \downarrow \rangle$ of the density matrix $\rho_s = |\psi_{q_x}\rangle \langle \psi_{q_x}|_s$ of the spin. In general, the scattering neutrinos will scatter with a distribution of momenta, so that there will be a mixed state density matrix, while the process itself will lead to a decoherence as well. We will therefore treat the evolution in terms of open quantum systems techniques, deriving a master equation to be followed by the density matrix.

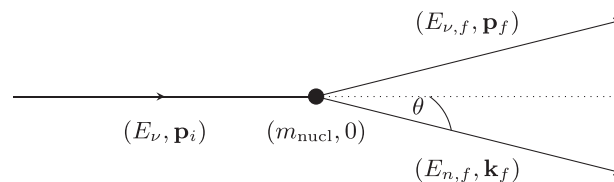


FIG. 2. Elastic scattering illustration with the scattering angle denoted as θ , the initial momenta p_i, k_i and the final momenta p_f, k_f .

III. COHERENT ELASTIC NEUTRINO-NUCLEUS SCATTERING CROSS SECTION

In this section, we discuss the CE ν NS cross section in the regime of reactor antineutrinos, since the calculation of the matrix element is directly related to the interaction Hamiltonian. For this purpose, we outline the description of coherent elastic scattering of a neutrino with incident four-momentum $p_i = (E_\nu, \mathbf{p}_i)$ by a nucleus of mass m_{nucl} and incident four-momentum $k_i = (m_{\text{nucl}}, 0)$, restricting ourselves to neutral current processes for the reason of simplicity. An illustration of the process is depicted in Fig. 2, where we have assumed the comparably heavy nucleus to be at rest and the final momenta to be of the form $p_f = (E_{\nu, f}, \mathbf{p}_f)$ and $k_f = (E_{n, f}, \mathbf{k}_f)$.

The incoming and outgoing four momenta can be reformulated in terms of the incoming neutrino energy E_ν , the kinetic energy transferred due to scattering T and the nucleus mass m_{nucl} ,

$$p_i = (E_\nu, \mathbf{p}_i), \quad (7)$$

$$k_i = (m_{\text{nucl}}, 0), \quad (8)$$

$$p_f = (E_\nu - T, \mathbf{p}_f), \quad (9)$$

$$k_f = (m_{\text{nucl}} + T, \mathbf{k}_f). \quad (10)$$

The tree-level Feynman diagram representing such a process is shown in Fig. 3.

To recover the cross section, the standard approach is to determine the scattering amplitude $\mathcal{M}_{s_s'}$ using the neutral current interaction Lagrangian

$$\mathcal{L} = \frac{G_F}{\sqrt{2}} J_\nu^\mu J_{\mu, \text{nucl}} \quad (11)$$

and the relevant Feynman rules [44]. The quantities described by J_ν^μ and $J_{\mu, \text{nucl}}$ denote the neutral currents of neutrino and

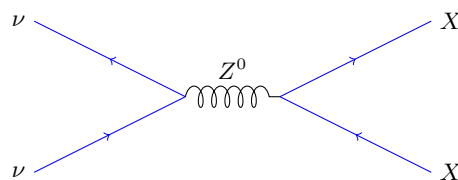


FIG. 3. Feynman diagram for neutral current coherent elastic ν -nucleus scattering, where time runs vertically. The label ν refers to the neutrino whereas the symbol X represents the nucleus.

nucleus. Neutral fermionic currents are given by

$$J_f^\mu = \sum_i \bar{\psi}_{f_i} \gamma^\mu (g_V^i - g_A^i \gamma^5) \psi_{f_i}, \quad (12)$$

where ψ_f denote the respective fermionic fields. Omitting the sum and inserting its couplings $g_V^v = 1/2$ and $g_A^v = 1/2$, the neutrino neutral current is

$$J_\nu^\mu = \bar{\psi}_\nu \gamma^\mu \frac{1}{2} (1 - \gamma^5) \psi_\nu. \quad (13)$$

It is a general feature of the weak interaction that its exchange bosons couple only to left-handed neutrinos or right-handed antineutrinos. For the nucleus neutral current, we choose a description in terms of its weak coupling constant and the four-momenta k_i, k_f ,

$$J_{\mu, \text{nucl}} = \frac{Q_W}{2} F(q^2) (k_i + k_f)_\mu, \quad (14)$$

where Q_W refers to the weak charge and $F(q)$ to the form factor dependent on the exchanged momentum q . Equation (11) can now be used to recover the Feynman amplitude \mathcal{M} , which is then formulated as follows

$$i\mathcal{M}_{ss'} = i \frac{G_F Q_W F(q^2) g_L^v}{\sqrt{2}} \times \bar{u}^{s'}(p_f) \gamma^\mu (1 - \gamma^5) \times u^s(p_i) (k_i + k_f)_\mu. \quad (15)$$

In the laboratory frame, the differential cross section with respect to the transferred kinetic energy is related to the absolute square of the matrix element as $\frac{d\sigma}{dT} = \frac{\sum_{ss'} |i\mathcal{M}_{ss'}|^2}{32\pi m_{\text{nucl}} E_\nu}$ and hence given by [45]

$$\frac{d\sigma}{dT} = \frac{G_F^2 Q_W^2 |F(q^2)|^2 m_{\text{nucl}}}{4\pi} \left(1 - \frac{T}{E_\nu} - \frac{m_{\text{nucl}} T}{2E_\nu^2} \right). \quad (16)$$

The differential cross section for the scattering of antineutrinos is derived analogously. Assuming a scattering angle θ between the initial neutrino and final nucleus momenta, the kinetic energy T can be expressed as follows:

$$T = \frac{2m_{\text{nucl}} E_\nu^2 \cos^2 \theta}{(m_{\text{nucl}} + E_\nu)^2 - E_\nu^2 \cos^2 \theta}. \quad (17)$$

The maximum kinetic energy transfer is then obtained for $\theta = 0$. The coherent elastic neutrino-nucleus cross section can be recovered from Eq. (16), following integration over kinetic energy. In all further calculations, we have approximated the form factor as $F(q) \sim 1$. This is appropriate solely for the energy range considered, since interactions involving higher neutrino-energies and therefore higher momentum transfers may be able to resolve the nucleus and eventually result in a suppression and flattening of the coherent cross-section. It should be noted that the cross section increases not only with neutrino energy, but also with increasing number of neutrons N in the target nucleus. The latter dependency becomes evident through a closer inspection of the weak charge

$$Q_W = [(1 - 4 \sin^2 \theta_W) Z + N]. \quad (18)$$

For the purpose of a real-world experiment, this means that the target material does play an important role in the

detectability of any scattering phase effect from neutrino scattering on nuclei.

IV. QUANTUM OPEN SYSTEMS AND THE BORN-MARKOV APPROXIMATION

We consider the scenario of a heavy nucleus in the presence of a (fermionic) bath of neutrinos scattering from it. As we have no control over a specific scattered neutrino, but nonetheless wish to describe the evolution of a comparably heavy nucleus, we resort to an open quantum systems approach. Following the description in Ref. [46], the total Hamiltonian of a weakly interacting system and bath is

$$H = H_S + H_B + H_{SB}, \quad (19)$$

where H_{SB} refers to the interaction between S and B . To derive the master equation of the system, it is of convenience to write the interaction Hamiltonian as

$$H_{SB} = \sum_\alpha S_\alpha B_\alpha, \quad (20)$$

with S_α and B_α denoting the system and bath operators. We will hence have to map the respective parts of our nonstandard interaction Hamiltonian for coherent elastic neutrino-nucleus scattering onto system and bath operators. The summation will become an integral over all relevant external three momenta. It shall also be noted that we impose hermiticity on H_{SB} . Taking the bath correlation time to be much shorter than the timescale over which our system evolves, we resort to a description in the Born-Markov approximation. The master equation for the system is then governed by

$$\frac{d\rho_S}{dt} = -\frac{i}{\hbar} [H_S, \rho_S] - \left\{ \int_0^\infty d\tau \sum_{\alpha\beta} C_{\alpha\beta}(-\tau) \times [S_\alpha S_\beta(-\tau) \rho_S - S_\beta(-\tau) \rho_S S_\alpha] + \text{H.c.} \right\}, \quad (21)$$

where

$$C_{\alpha\beta} = \frac{1}{\hbar^2} \text{Tr}[\rho_B B_\alpha B_\beta(-\tau)] \quad (22)$$

is the bath correlation function and the time dependence of the operators S_β and B_β is determined by

$$S_\beta(-\tau) = e^{-\frac{iH_S\tau}{\hbar}} S_\beta e^{\frac{iH_S\tau}{\hbar}}, \quad (23)$$

$$B_\beta(-\tau) = e^{-\frac{iH_B\tau}{\hbar}} B_\beta e^{\frac{iH_B\tau}{\hbar}}. \quad (24)$$

As we work in natural units, we set $\hbar = c = 1$ for now.

A. Quantum master equation for neutrino-nucleus scattering

The Lagrangian density [47] for the interaction of neutrino ν and nucleus n is given by Eq. (11). Hence, the interaction Hamiltonian $H_{n,\nu}$ corresponds to

$$\begin{aligned} H_{n,\nu} &= - \int d^3x \mathcal{L}(x) \\ &= - \frac{G_F}{\sqrt{2}} \int d^3x J_\nu^\mu(x) J_{\mu, \text{nucl}}(x) = H_{SB}. \end{aligned} \quad (25)$$

Choosing to rewrite the neutrino current in second quantized form, we observe that

$$\begin{aligned} J_v^\mu(x) &= \bar{\psi}_v(x) \frac{1}{2} \gamma^\mu (1 - \gamma^5) \psi_v(x) \\ &= \int \frac{d^3 p_i d^3 p_f}{(2\pi)^6 \sqrt{4E_{p_i} E_{p_f}}} a_{p_f}^\dagger a_{p_i} e^{-i(p_i - p_f)x} \bar{u}^2(p_f) \frac{1}{2} \gamma^\mu (1 - \gamma^5) u^2(p_i), \end{aligned} \quad (26)$$

so that our Hamiltonian is

$$H_{n,v} = - \frac{G_F Q_W F(q)}{2\sqrt{2}} \int d^3 x \frac{d^3 p_i d^3 p_f d^3 k_i d^3 k_f}{(2\pi)^{12} \sqrt{16E_{p_i} E_{p_f} E_{k_i} E_{k_f}}} e^{-i(k_i + p_i - k_f - p_f)x} a_{p_f}^\dagger a_{p_i} \bar{u}^s(p_f) \gamma^\mu (1 - \gamma^5) u^s(p_i) c_{k_f}^\dagger c_{k_i} (k_f + k_i)_\mu. \quad (27)$$

Note that although here we have generically used k_i, k_f to label 3-momenta, $(k_f + k_i)_\mu$ stand for 4-momenta. Noting that the only x -dependence is now in the exponential, we can perform the spatial integration. Further to this, the factor $F(q) \sim 1$ in our scenario and can therefore be neglected,

$$\begin{aligned} H_{n,v} &= - \frac{(2\pi)^3 G_F Q_W}{2\sqrt{2}} \int \frac{d^3 p_i d^3 p_f d^3 k_i d^3 k_f}{(2\pi)^{12} \sqrt{16E_{p_i} E_{p_f} E_{k_i} E_{k_f}}} \delta^3(k_i + p_i - k_f - p_f) a_{p_f}^\dagger a_{p_i} \bar{u}^s(p_f) \gamma^\mu (1 - \gamma^5) u^s(p_i) c_{k_f}^\dagger c_{k_i} (k_f + k_i)_\mu \\ &= \frac{(2\pi)^3 G_F Q_W}{2\sqrt{2}} \int \frac{d^3 p_i d^3 p_f d^3 k_i d^3 k_f}{(2\pi)^{12} 16E_{p_i} E_{p_f} E_{k_i} E_{k_f}} \bar{u}^s(p_f) \gamma^\mu (1 - \gamma^5) u^s(p_i) (k_f + k_i)_\mu \delta^3(k_i + p_i - k_f - p_f) |p_f\rangle \langle p_i| \otimes |k_f\rangle \langle k_i|, \end{aligned} \quad (28)$$

with one-particle states $|p, s\rangle = \sqrt{2E_p} a_p^{s\dagger} |0\rangle$. In Eq. (28), we have treated the nucleus and neutrino as single particles and applied a mapping to suitable momentum-basis states. Using the matrix element for the neutrino-nucleus scattering $\mathcal{M}_{p_i, k_i, p_f, k_f} = \frac{G_F Q_W}{2\sqrt{2}} \bar{u}^s(p_f) \gamma^\mu (1 - \gamma^5) u^s(p_i) (k_f + k_i)_\mu$ and by computing the integral over the final nucleus momentum k_f we get

$$\begin{aligned} \hat{H}_{n,v} &= \int \frac{d^3 p_i d^3 p_f d^3 k_i d^3 k_f}{(2\pi)^9 2E_{p_i} 2E_{p_f} 2E_{k_i} 2E_{k_f}} \mathcal{M}_{p_i, k_i, p_f, k_f} \delta^3(k_i + p_i - k_f - p_f) |p_f\rangle \langle p_i| \otimes |k_f\rangle \langle k_i| \\ &= \int \frac{d^3 p_i d^3 p_f d^3 k_i \mathcal{M}_{p_i, k_i, p_f, k_i + p_i - p_f}}{(2\pi)^9 2E_{p_i} 2E_{p_f} 2E_{k_i} 2E_{k_i + p_i - p_f}} |p_f\rangle \langle p_i| \otimes |k_i + p_i - p_f\rangle \langle k_i| \\ &= \int \frac{d^3 p_i d^3 p_f d^3 k_i \mathcal{M}_{p_i, k_i, p_f, k_i + p_i - p_f}}{(2\pi)^9 2E_{p_i} 2E_{p_f} 2E_{k_i} 2E_{k_i + p_i - p_f}} |p_f\rangle \langle p_i| \otimes e^{i(p_i - p_f)\hat{x}} |k_i\rangle \langle k_i|, \end{aligned} \quad (29)$$

where we have used the fact that the momentum state $|k_i + p_i - p_f\rangle$ can be rewritten in a suitable manner. Now we make a crucial simplifying approximation: we assume the nucleus mass to be sufficiently large compared to its momenta $m_{\text{nuc}} \gg |k|$. Being inside the crystal which is stationary, we treat the nucleus as being effectively at rest so that the expression of the matrix element implies $\mathcal{M}_{p_i, k_i, p_f, k_f} \sim \mathcal{M}_{p_i, 0, p_f, 0}$. Let us write the nucleus integrals explicitly, so that $d\mu_v$ now only comprises the neutrino momentum integrals,

$$\begin{aligned} \hat{H}_{n,v} &= \int d\mu_v \int d^3 k_i \frac{\mathcal{M}_{p_i, 0, p_f, 0}}{(2\pi)^3 (2E_{k_i} 2E_{k_i + p_i - p_f})} \\ &\quad \times |p_f\rangle \langle p_i| \otimes e^{i(p_i - p_f)\hat{x}} |k_i\rangle \langle k_i|. \end{aligned} \quad (30)$$

For a very heavy nucleus, let us further assume that we can approximate the quantity $2E_{k_i} 2E_{k_i + p_i - p_f} \sim 4m_{\text{nuc}} E_{k_i}$. Seeing as the difference in the neutrino momenta is small and the energy of the nucleus is predominantly dependent on its heavy mass, we take this to be a reasonable justification for the model at hand. As a consequence, we observe that the Hamiltonian reduces further, for we are now able to use the definition for the one-particle state identity resolution,

$$\hat{H}_{n,v} = \int d\mu_v \frac{\mathcal{M}_{p_i, p_f}}{2m_{\text{nuc}}} |p_f\rangle \langle p_i| \otimes e^{i(p_i - p_f)\hat{x}} \mathbb{I}. \quad (31)$$

Next, we associate the operators of the bath with the integrals over the amplitudes, whereas the rest of the above Hamiltonian is kept in the system operators. In our case, we identify

$$S_\alpha = \frac{1}{2m_{\text{nuc}}} e^{i(p_i - p_f)\hat{x}} \mathbb{I}, \quad B_\alpha = \mathcal{M}_{p_i, p_f} |p_f\rangle \langle p_i|, \quad (32)$$

and we pack all dependencies on the Feynman amplitudes into the bath operators. Further, we argue that the COM of the crystal (to which the nucleus belongs) is trapped in a very low frequency trap, so that the time evolution of the operator S_β can be neglected. To time evolve the neutrino state, we assume the neutrino rest mass to be negligible with respect to its total energy. We further neglect flavor oscillations, which is a reasonable assumption over the short distances of $d \sim 20$ m we consider, so that the neutrino bath has the free Hamiltonian

$$H_B = \int \frac{d^3 p}{(2\pi)^3} E_p a_p^\dagger a_p. \quad (33)$$

At first we will consider a single neutrino scattering from the nucleus, thus we need to find the bath correlation function for a single neutrino bath. To do that, we need to use an incoming neutrino in a sufficiently momentum localized state $|\psi\rangle$ normalized to $\langle\psi|\psi\rangle = 1$. This is achieved by starting

with a generic Gaussian initial momentum state,

$$\begin{aligned}
 |\psi\rangle &= \int \frac{d^3 p}{(2\pi)^3 \sqrt{2E_p}} \psi(p) |p\rangle \\
 &= \int \frac{d^3 p}{(2\pi)^3 \sqrt{2E_p}} \frac{(2\pi)^{3/2}}{(2\pi\sigma^2)^{3/4}} e^{-\frac{(p-p_0)^2}{4\sigma^2}} |p\rangle. \quad (34)
 \end{aligned}$$

We substitute $\tilde{\sigma} = \sqrt{2}\sigma$, such that our state is properly normalized to $\langle\psi|\psi\rangle = 1$ and regard it in the limit of a very

narrow wave function,

$$\begin{aligned}
 \lim_{\tilde{\sigma} \rightarrow 0} |\psi\rangle &= \lim_{\tilde{\sigma} \rightarrow 0} \int \frac{d^3 p (4\pi\tilde{\sigma}^2)^{3/4} e^{-\frac{(p-p_0)^2}{2\tilde{\sigma}^2}}}{(2\pi)^{3/2} \sqrt{2E_p} (2\pi\tilde{\sigma}^2)^{3/2}} |p\rangle \\
 &= \epsilon \int \frac{d^3 p}{\sqrt{2E_p}} (\tilde{\sigma})^{3/2} \delta^3(p - p_0) |p\rangle \\
 &= \frac{\epsilon \tilde{\sigma}^{3/2}}{\sqrt{2E_{p_0}}} |p_0\rangle. \quad (35)
 \end{aligned}$$

Here, ϵ represents the collected numerical factors. We will use this simplified form in the last step above for our subsequent computations. Thus,

$$\begin{aligned}
 C_{\alpha,\beta} &= Tr[\rho_\nu B_\alpha B_\beta(-\tau)] \\
 &= Tr[|\psi\rangle\langle\psi| \mathcal{M}_{p_i,p_f} \mathcal{M}_{p'_f,p'_i}^* e^{-i(E_{p'_i}-E_{p'_f})\tau} |p_f\rangle\langle p_i| p'_f\rangle\langle p'_i|] \\
 &= (2\pi)^3 \mathcal{M}_{p_i,p_f} \mathcal{M}_{p'_f,p'_i}^* 2E_{p_i} \delta^3(p_i - p'_f) \langle\psi|\psi\rangle \langle\psi| e^{-i(E_{p'_i}-E_{p'_f})\tau} |p_f\rangle\langle p'_i|\psi\rangle \\
 &= (2\pi)^3 \mathcal{M}_{p_i,p_f} \mathcal{M}_{p'_f,p'_i}^* 2E_{p_i} \delta^3(p_i - p'_f) \langle\psi| e^{-i(E_{p'_i}-E_{p'_f})\tau} |p_f\rangle\langle p'_i|\psi\rangle \\
 &= (2\pi)^9 \epsilon^2 \tilde{\sigma}^3 \mathcal{M}_{p_i,p_f} \mathcal{M}_{p'_f,p'_i}^* 2E_{p_i} \delta^3(p_i - p'_f) e^{-i(E_{p'_i}-E_{p'_f})\tau} 2E_{p'_i} \delta^3(p_0 - p_f) \delta^3(p'_i - p_0). \quad (36)
 \end{aligned}$$

In tracing over the neutrino's degrees of freedom, we have obtained the bath correlation function $C_{\alpha,\beta}$ as a function of the relevant neutrino momenta, with α and β , respectively, labeling the dashed and undashed momenta. We then proceed to insert the expression into the general formula for the master equation. For $d\rho_S/dt$ this results in the second term of Eq. (21) given by

$$\begin{aligned}
 \frac{d\rho_S}{dt} &= -\frac{\epsilon^2 \tilde{\sigma}^3}{4m_{\text{nucl}}^2} \int d\tau \int \frac{d^3 p_i d^3 p_f d^3 p'_i d^3 p'_f}{(2\pi)^3 16E_{p_i} E_{p_f} E_{p'_i} E_{p'_f}} 4E_{p_i} E_{p'_i} \mathcal{M}_{p_i,p_f} \mathcal{M}_{p'_f,p'_i}^* \delta^3(p_i - p'_f) \\
 &\quad \times e^{-i(E_{p'_i}-E_{p'_f})\tau} \delta^3(p_0 - p_f) \delta^3(p'_i - p_0) \{-e^{i(p'_i-p'_f)\hat{x}} \rho_S e^{i(p_i-p_f)\hat{x}} + e^{i(p_i-p_f)\hat{x}} e^{i(p'_i-p'_f)\hat{x}} \rho_S + \text{H.c.}\} \\
 &= -\frac{\epsilon^2 \tilde{\sigma}^3}{4m_{\text{nucl}}^2} \int d\tau \int \frac{d^3 p_f d^3 p'_i d^3 p'_f}{(2\pi)^3 4E_{p_f} E_{p'_f}} \mathcal{M}_{p'_f,p_f} \mathcal{M}_{p'_f,p'_i}^* e^{-i(E_{p'_i}-E_{p'_f})\tau} \delta^3(p_0 - p_f) \\
 &\quad \times \delta^3(p'_i - p_0) \{-e^{i(p'_i-p'_f)\hat{x}} \rho_S e^{i(p'_f-p_f)\hat{x}} + e^{i(p'_f-p_f)\hat{x}} e^{i(p'_i-p'_f)\hat{x}} \rho_S + \text{H.c.}\} \\
 &= -\frac{\epsilon^2 \tilde{\sigma}^3}{8m_{\text{nucl}}^2 E_{p_0}} \int d\tau \frac{d^3 p'_f}{(2\pi)^3 2E_{p'_f}} |\mathcal{M}_{p_0,p'_f}|^2 e^{-i(E_{p_0}-E_{p'_f})\tau} \{-e^{i(p_0-p'_f)\hat{x}} \rho_S e^{i(p'_f-p_0)\hat{x}} + e^{i(p'_f-p_0)\hat{x}} e^{i(p_0-p'_f)\hat{x}} \rho_S + \text{H.c.}\}. \quad (37)
 \end{aligned}$$

Last, we have

$$\begin{aligned}
 \frac{d\rho_S}{dt} &= -\frac{\epsilon^2 \tilde{\sigma}^3}{64\pi^2 m_{\text{nucl}}^2 E_{p_0}} \int \frac{d^3 p'_f}{E_{p'_f}} |\mathcal{M}_{p_0,p'_f}|^2 \\
 &\quad \times \delta(E_{p_0} - E_{p'_f}) \{-e^{i(p_0-p'_f)\hat{x}} \rho_S e^{i(p'_f-p_0)\hat{x}} \\
 &\quad + e^{i(p'_f-p_0)\hat{x}} e^{i(p_0-p'_f)\hat{x}} \rho_S + \text{c.c.}\}. \quad (38)
 \end{aligned}$$

It is always possible to find a suitable parametrization of the momenta p_0 and p'_f in terms of an energy and appropriate angles. Therefore, $\mathcal{M}_{p_0,p'_f} = \mathcal{M}(E_{p'_f}, \Omega) \equiv \mathcal{M}(\Omega)$. Setting $\alpha = \frac{\epsilon^2 \tilde{\sigma}^3}{64\pi^2 m_{\text{nucl}}^2}$ for brevity, we are able to write the factor before

the curly brackets as

$$\begin{aligned}
 \Gamma &= -\alpha \int \frac{E_{p'_f}^2 dE_{p'_f} d\Omega}{E_{p_0} E_{p'_f}} |\mathcal{M}(E_{p'_f}, \Omega)|^2 \delta(E_{p_0} - E_{p'_f}) \\
 &= -\frac{\epsilon^2 \tilde{\sigma}^3}{64\pi^2 m_{\text{nucl}}^2} \int d\Omega |\mathcal{M}(\Omega)|^2. \quad (39)
 \end{aligned}$$

It shall be noted that the factor $\epsilon^2 \tilde{\sigma}_p^3 = 2^{-\frac{3}{2}} (2\pi \tilde{\sigma}_x^2)^{-\frac{3}{2}} = (2\pi \sigma_x^2)^{-\frac{3}{2}} = V_x^{-1}$ is essentially the volume of a Gaussian times a factor. Seeing as $\sigma_x = (\int x^2 |\psi(x)|^2 dx)^{1/2}$ for a conventionally normalized $\psi(x)$, our normalized Gaussian in position space yields the recovered prefactor. The prefactor can be interpreted as the expectation value of finding a particle within the volume element V_x , which implies that number of particles per unit volume $n = 1/V_x$. The neutrino's velocity

$|p_\nu|/E_\nu \sim c = 1$. Hence, its flux is given by

$$F = nc = n, \quad (40)$$

where n is the number of particles per unit volume. We have normalized the single neutrino wave function to 1 particle per unit volume. Thus, we have, in terms of the flux of 1 particle, F_1 , the evolution of the reduced density matrix of the nucleus as given by

$$\frac{d\rho_S}{dt} = -\frac{F_1}{64\pi^2 m_{\text{nuc}}^2} \int d\Omega |\mathcal{M}(\Omega)|^2 \times \left\{ -e^{i\Delta(E_0, \Omega)\hat{x}} \rho_S e^{-i\Delta(E_0, \Omega)\hat{x}} + \rho_S + \text{c.c.} \right\}, \quad (41)$$

and hence

$$\langle x | \dot{\rho}_S | y \rangle = -\frac{2F_1}{64\pi^2 m_{\text{nuc}}^2} \int d\Omega |\mathcal{M}(\Omega)|^2 \times \left\{ -e^{i\Delta(E_0, \Omega)(x-y)} + 1 \right\} \langle x | \rho_S | y \rangle. \quad (42)$$

In writing the above, we have implicitly assumed that the system, i.e., the nucleus, has a negligible evolution due to its own Hamiltonian H_S during the timescale of the experiment. In addition, we have labeled $E_{p_0} \equiv E_0$.

We are now in a position to compute the change in the density matrix of the center of mass of the whole crystal which is composed of multiple nuclei subject to a large flux of neutrinos from a reactor. It shall be noted that our approximations yield a result which is qualitatively very close to the form of Gallis-Fleming [48] for nonrelativistic particles scattering from a mass. Moreover, Eq. (42) has a very intuitive interpretation, with $\frac{F_1}{64\pi^2 m_{\text{nuc}}^2} d\Omega |\mathcal{M}(\Omega)|^2$ being the incident flux multiplied by the scattering cross section for a solid angle $d\Omega$. It is thus the rate of scattering in a given solid angle $d\Omega$. Each scattering direction $d\Omega$ imparts a different momentum to the nucleus, which is given by the operator $e^{i\Delta(E_0, \Omega)\hat{x}}$.

B. Calculation of the relative phase between superposed components of a crystal and its detection

For our formalism to apply to a whole crystal in the form of a bulk material consisting of multiple nuclei scaling as N_{Atoms} and a flux of incoming neutrinos with a spectral distribution of energies $S(E)$, Eq. (42) will have to be modified to

$$\frac{d\rho_S}{dt} = -\frac{2F_1 \times N_{\text{Atoms}}}{64\pi^2 m_{\text{nuc}}^2} \int dES(E) \int d\Omega |\mathcal{M}(\Omega)|^2 \times \left\{ -e^{i\Delta(E, \Omega)\hat{x}} \rho_S e^{-i\Delta(E, \Omega)\hat{x}} + \rho_S + \text{c.c.} \right\}. \quad (43)$$

Antineutrino production rates for nuclear reactor sources are typically on the order of $r \sim 2 \times 10^{20} \text{ s}^{-1}/\text{GW}_{\text{th}}$ [50,51], with antineutrino energies ranging from 1–10 MeV. Seeing as we assume our detectors to be placed at a distance $d = 20 \text{ m}$ to a 4.5 GW_{th} nuclear fission reactor source, we obtain an estimated flux of

$$F_1 = \frac{r_{4.5 \text{ GW}_{\text{th}}}}{4\pi d^2} \sim 1.7 \times 10^{13} \text{ cm}^{-2}\text{s}^{-1}. \quad (44)$$

As described earlier, the center of mass C of the crystal will be initialized in a joint state with its spin s , in the motional superposition state $|\Psi_0\rangle_S = \frac{1}{\sqrt{2}}(|\uparrow\rangle_s |\bar{x}_0\rangle_C + |\downarrow\rangle_s |\bar{x}_1\rangle_C)$.

Labeling the orthonormal states $|\uparrow\rangle_s |\bar{x}_0\rangle_C$ and $|\downarrow\rangle_s |\bar{x}_1\rangle_C$ with $|0\rangle$ and $|1\rangle$, respectively, for simplicity, we get the initial density matrix in the $\{|0\rangle, |1\rangle\}$ basis as

$$\rho_0 = \frac{1}{2} \begin{pmatrix} 1 & 1 \\ 1 & 1 \end{pmatrix}. \quad (45)$$

As we have discussed, for low momentum transfer with respect to the inverse of the width of the Gaussians \bar{x}_0 and \bar{x}_1 , they can be treated effectively as position eigenstates $|\bar{x}_0\rangle$ and $|\bar{x}_1\rangle$ in the phase expression. Thus, the evolution of the density matrix in a time Δt , which we call the final density matrix ρ_f is given by

$$\begin{aligned} \langle 0 | \rho_f | 1 \rangle &= \langle 0 | \rho_S(\Delta t) | 1 \rangle = \langle 0 | \rho_S(0) | 1 \rangle \\ &- \frac{2F_1 \times N_{\text{Atoms}}}{64\pi^2 m_{\text{nuc}}^2} \int dES(E) \int d\Omega |\mathcal{M}(\Omega)|^2 \\ &\times \left\{ -e^{i\Delta(E, \Omega)(\bar{x}_0 - \bar{x}_1)} + 1 \right\} \langle 0 | \rho_S(0) | 1 \rangle \Delta t. \end{aligned} \quad (46)$$

We then split the solid angle integration into polar and azimuthal integrals over φ and θ and choose the parametrization of the problem such that $\Delta(E, \Omega) = E(1 - \cos \theta)$. As a result of the above evolution, we will obtain a final density matrix of the general form

$$\rho_f = \begin{pmatrix} a & Ae^{-i\varphi} \\ Ae^{i\varphi} & b \end{pmatrix}, \quad (47)$$

in terms of a phase φ and an amplitude A . Unlike in the case of a simple phase acquisition, the amplitude accompanying the off diagonal term of the density matrix, where the phase is encoded, has also decayed because of the open systems treatment. In other words, we are averaging over all angles of scattering, which amounts to averaging over all momenta and incident energies. To extract the effect of the scattering, the center of mass C will be decoupled using the interferometry methods described in Refs. [24,25]. The relative phase acquired between $|\uparrow\rangle_s |\bar{x}_0\rangle_C$ and $|\downarrow\rangle_s |\bar{x}_1\rangle_C$ will appear between spin states $|\uparrow\rangle_s$ and $|\downarrow\rangle_s$ and be measured after suitable transformations between them. At the end of interferometry, $|\uparrow\rangle_s |\bar{x}_0\rangle_C$ and $|\downarrow\rangle_s |\bar{x}_1\rangle_C$ are mapped to spin states $|\uparrow\rangle_s$ and $|\downarrow\rangle_s$, respectively, and we can continue to use $|0\rangle$ and $|1\rangle$ as our basis with the understanding that these now refer to the spin states $|\uparrow\rangle_s$ and $|\downarrow\rangle_s$ which are measured. Unitary operations on spin states typically comprise sending microwave pulses of appropriate frequencies to spin states [40] differing in energies due to the Zeeman effect in an external magnetic field, hyperfine interactions or crystal field anisotropies. The entire toolbox of quantum computation is available and we will use two quantum operations, the Hadamard gate H and the phase gate S [52], on the spins before measuring the populations of $|\uparrow\rangle_s$ and $|\downarrow\rangle_s$.

After computing $\rho_f(x_1, x_2, t)$, upon applying a Hadamard transformation, we effectively rotate our bases from $|0\rangle \rightarrow \frac{1}{\sqrt{2}}(|0\rangle + |1\rangle)$ and $|1\rangle \rightarrow \frac{1}{\sqrt{2}}(|0\rangle - |1\rangle)$. The extraction of the phase then becomes a matter of calculating the probabilities of measuring $|0\rangle\langle 0|$ or $|1\rangle\langle 1|$. For the final density matrix a Hadamard transformation to the rotated basis yields

$$H\rho_f H = \frac{1}{2} \begin{pmatrix} a + b + 2A \cos \varphi & a - b + 2iA \sin \varphi \\ a - b - 2iA \sin \varphi & a + b - 2A \cos \varphi \end{pmatrix}, \quad (48)$$

TABLE I. Constants and definitions. G_F denotes the Fermi constant, u the atomic mass unit, m_{nuc} the mass of a nucleus. The flux listed is the projected neutrino flux at a distance of 20 m from the source and Δx refers to the superposition size. The function $S(E)$ is a spectral distribution function over the energies E , with standard deviation σ_E and mean energy E_0 .

G_F	$1.1664 \times 10^{-11} [\text{MeV}^{-2}]$
u	$931.5 [\text{MeV} \cdot \text{c}^{-2}]$
m_{nuc} [49]	$(Z + N)u - 0.00054858Z \cdot u + (14.4381Z^{2.39} + 1.55468 \cdot 10^{-6}Z^{5.35})10^{-6}$
Flux	$1.7 \cdot 10^{13} [\text{s} \cdot \text{cm}^{-2}]$
Δx	$10^{-14} [\text{m}]$
$S(E)$	$\frac{1}{\sigma_E \sqrt{2\pi}} e^{-(E-E_0)^2/(2\sigma_E^2)}$
σ_E	$0.75 [\text{MeV}]$
E_0	$2.6 [\text{MeV}]$

and therefore subtraction of the probabilities $p(0) - p(1)$ results in

$$p(0) - p(1) = 2A \cos \varphi. \quad (49)$$

As it is sometimes more practical to express the phase for small arguments via the sine, a phase gate of the form

$$S = \begin{pmatrix} 1 & 0 \\ 0 & e^{i\pi/2} \end{pmatrix} \quad (50)$$

is used before the Hadamard transformation to recover

$$p_{S,H}(1) - p_{S,H}(0) = 2A \sin \varphi. \quad (51)$$

For a crystal consisting of $N_{\text{Atoms}} = 5 \times 10^{21}$ of the element ^{209}Bi (crystal mass $m \sim 1$ g) and the parameters as given in Table I, we observe phase accumulation and its amplitude decay in Fig. 4. From the figure it is clear that at time $\sim 10^5$ s, a very significant phase difference between the components of the superposition with a significant amplitude is obtained for a superposition of size $\Delta x = |\bar{x}_0 - \bar{x}_1| \sim 10^{-14}$ m. Reductions in the mass of the detector would linearly suppress

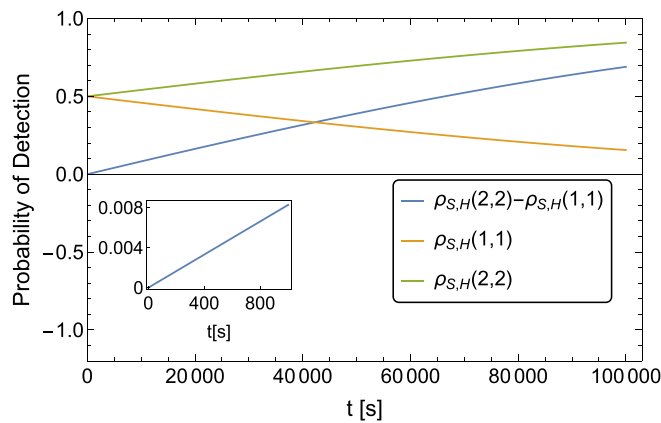


FIG. 4. Phase accumulation due to coherent neutrino-nucleus scattering from Bismuth. The figure depicts the normalized matrix elements of the nucleus density matrix after performing the operations of a phase gate and subsequent Hadamard on the sensing system. Most notably, the blue line shows the change resulting from the scattering in terms of the sine of the accumulated phase.

the associated phase and hence one would require a large number of detectors (see section V for more details). The separation was optimized and this order of magnitude was found to give a detectable phase with minimal damping at $\sim 10^5$ s. This timescale corresponds to a $\sim \pi/3 \sim 1$ phase shift. About thrice this time corresponds to a π phase shift as the phase growth is linear in time. For a π phase shift, if we can ensure that there has been no other momenta imparting particle/effect, then this corresponds to the detection of one neutrino by our detector with 100% certainty (a “click” in our detector) as such a phase is measured in a single shot by measuring the spin state in the $\{|+\rangle_s, |-\rangle_s\}$ basis with the outcome $|+\rangle_s$ corresponding to no neutrinos, and the outcome $|-\rangle_s$ corresponding to one neutrino. The chance of more than one neutrino scattering in the given timescale is exceptionally small. Smaller nonzero phases ascertained at earlier times using Eq. (51) and multiple measurements to determine probabilities (i.e., repeating the procedure with the same detector or conducting measurements on an array of detectors) will detect the neutrino stream coming from the reactor, but will not be a single shot “click” detector.

V. CREATION OF QUANTUM SUPERPOSITIONS OF MACROSCOPIC OBJECTS

We have three requirements for our setup. First, the crystal should stay suspended against gravity for the duration of $\sim 10^5$ s of our experiment, although we will outline methods of reducing this time by resorting to a detector array rather than a single detector. Using whatever means, we have to trap the object in the vertical z direction. This could be achieved via the well demonstrated mechanism of diamagnetic levitation which will balance the crystal against gravity. Once created, the quantum superposition of $m \sim 1$ g, $\Delta x \sim 10^{-14}$ m has to be kept coherent for 10^5 s. This is a very long time, but the principal mechanisms of decoherence are known [7], namely, the collisions with background gas (controlled by decreasing pressure) and black-body radiation emission from the crystal (controlled by cooling the crystal internally). Figure 5 shows the requirements, with the unshaded region (outside the red bounded box) an allowed domain for coherence. It shows that pressures of $P \sim 10^{-16}$ Pa, already achieved in penning traps, and temperatures of $T \sim 1$ K should suffice to retain the extremely long coherence for 10^5 s. The effect of electromagnetic noise from the apparatus to create and probe the superposition is also of importance (analysed to some extent in Ref. [24]) and depends on the precise protocol, but essentially the exceptional stability of these sources, along with other proximal electromagnetic sensors will have to be used. For inertial noise, again, other sensors will have to be used to measure and take account of the noise. Alternatively, the detection can be done with two different materials in parallel, with the inertial noise being common. An in-depth noise analysis including vibrational noise will be discussed in future works. The explicit development of the above are beyond the scope of the current work, where we just want to highlight the possibility of neutrino detection.

Methods for creating superpositions of the form $|\Psi_0\rangle = \frac{1}{\sqrt{2}}(|\uparrow\rangle_s |\bar{x}_0\rangle_C + |\downarrow\rangle_s |\bar{x}_1\rangle_C)$ are still in development. Of course, our method will work for superpositions created by

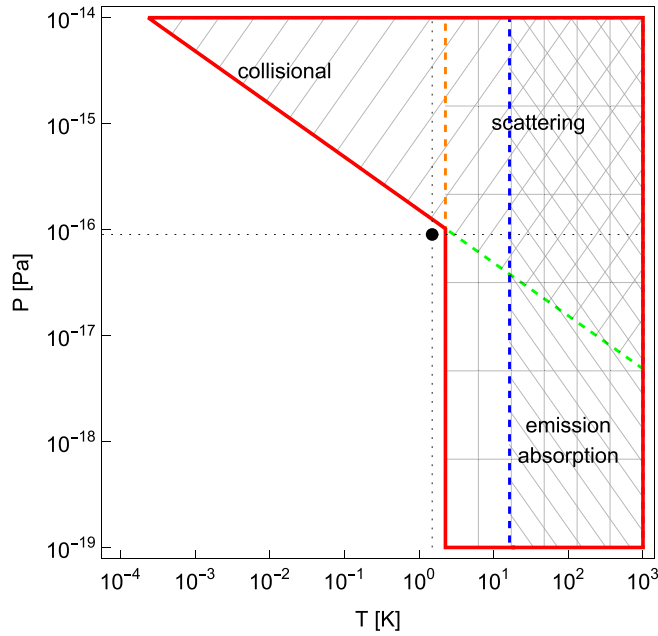


FIG. 5. The diagram of the allowable region of pressure P and temperature T so that a $m \sim 1$ g crystal in a superposition of two positions separated by $\Delta x \sim 10^{-14}$ m can remain coherent for a time $t \sim 10^5$ s. The allowable region is unshaded. We can see that $P \sim 10^{-16}$ Pa and $T \sim 1$ K (the black dot) is an optimal point for our scheme.

any means, even for superpositions without an ancillary spin system, such as $\frac{1}{\sqrt{2}}(|\bar{x}_0\rangle_C + |\bar{x}_1\rangle_C)$, as long as we have a mechanism to measure the relative phase between the components by bringing them together to interfere. It is just simpler for a superposition of the form $|\Psi_0\rangle = \frac{1}{\sqrt{2}}(|\uparrow\rangle_s|\bar{x}_0\rangle_C + |\downarrow\rangle_s|\bar{x}_1\rangle_C)$, as the spin can be measured after the completion of interferometry to measure the phase. Here we only outline schematics rather than fully detailed schemes. One can use a mass with a single quantum spin $-1/2$ system embedded in it and subject it to magnetic field gradients. The $m \sim 1$ g crystal with an embedded spin is subjected to a $\frac{\partial B}{\partial x} \sim 10^6$ Tm $^{-1}$ (produced, for example, at a \sim cm distance from the surface of a \sim cm radius wire [24] carrying 10^{13} A m $^{-2}$ current densities). When exposed to this magnetic field gradient for a time $t_{\text{acc}} \sim 10^{-5}$ s, the center of mass of the crystal acquires opposite final velocities of magnitude $v \sim \frac{\mu_B \frac{\partial B}{\partial x}}{m} \tau \sim 10^{-19}$ m s $^{-1}$ for the $|\uparrow\rangle$ and $|\downarrow\rangle$ components, respectively. It is not worth exposing the crystal to the high magnetic field gradient much longer as this gradient, in addition to the Stern-Gerlach splitting, also creates a diamagnetic trap of a frequency $\omega \sim \sqrt{\frac{\chi_m}{\mu_0} \frac{\partial B}{\partial x}} \sim 10^5$ Hz in the x direction, which reverses the directions of the opposite accelerations after a quarter period. After this, the x gradient is switched off, and the mass is allowed to freely evolve for the exceptionally long time $\tau \sim 10^5$ s of our experiment in the diamagnetic trap in the vertical z direction. Since there is no trapping/potential in the x direction, the velocity difference is translated to a position difference $\Delta x \sim 2v\tau \sim 10^{-14}$ m. Note that during the stages in which the Stern-Gerlach effect is not used to actively accelerate the crystal, the electronic spin

states used in the Stern-Gerlach splitting can be mapped on to nuclear spin states which maintain their quantum coherence for exceptionally long times [53].

Another method to create a quantum superposition will be through using an optomechanical interaction with a quantized microwave field in a cavity, with the cavity field subsequently mapped to spin qubits. In this case, the optomechanical force is sufficient to create the required superposition of a single $m \sim 1$ g mass directly. An electromagnetic field in a number state $|n\rangle$ in a cavity interacts with a crystal passing through it with the coupling strength $g \sim \frac{3V}{4V_c} \frac{\epsilon-1}{\epsilon+1} \omega_L$, where ω_L is the frequency of the electromagnetic field, V is the volume of the crystal, and V_c is the cavity waist volume and ϵ the dielectric constant [54]. The optomechanical coupling Hamiltonian is $\hbar g k \hat{n} \hat{x}$, where \hat{n} and \hat{x} are the number and the position operators of the field and the center of mass of the crystal, respectively, and k is the wave vector of the electromagnetic field. If interacting for a time t_{kick} , then a crystal can receive a velocity kick $v_{\text{kick}} \sim \frac{\hbar g k n t_{\text{kick}}}{m}$. Assuming a $t_{\text{kick}} \sim 1$ μ s during which the 1 g mass traverses through the cavity waist, assuming both $V \sim V_c \sim 1$ cm 3 and $\omega_L \sim 10$ GHz, we get a velocity kick of $v_{\text{kick}} \sim 10^{-19}$ ms $^{-1}$. Thus, one can prepare the cavity in a quantum superposition $\frac{1}{\sqrt{2}}(|0\rangle_c + |1\rangle_c)$ and apply a kick to the crystal by letting it fall through the cavity for t_{kick} . After waiting for a time $\tau \sim 10^5$ s, one obtains a superposition $\frac{1}{\sqrt{2}}(|0\rangle_c |\bar{x}_0\rangle_C + |1\rangle_c |\bar{x}_1\rangle_C)$ [4]. The microwave cavity state can also be mapped to a long-lived nuclear spin states of trapped atoms after the state dependent velocity kicks are over.

Whatever the mechanism of trapping the masses and creating the spatial superpositions, randomness of the forces and pulses will also result in a decoherence at a rate of

$$\Gamma \sim \frac{S_{FF}(\Omega)(\Delta x)^2}{\hbar^2}, \quad (52)$$

where $S_{FF}(\Omega) = \int \delta F(0) \delta F(t) e^{i\Omega t} dt$ is the force noise spectrum at the frequency $\Omega \sim 1/\tau$ of our experiment. Keeping $\Gamma < 10^{-5}$ Hz gives us the constraint that random force noise should be kept below $\sqrt{S_{FF}} \sim 10^{-23}$ N/ $\sqrt{\text{Hz}}$. Note that in all the above discussions, it is implicit that the interferometry has to be completed. So further spin or cavity field dependent impulses will be required at certain points to stop the growth of Δx and reverse it, as it is accomplished in various interferometric schemes [24,25].

Note that the phase growth between the components of the superposition when subject to a neutrino flux is linear with time at a constant rate of $\sim 10^{-5}$ Hz, which reflects in population differences as seen from Fig. 4. At $\sim 10^5$ s, the phase difference of the order π is obtained so that the final state of the superposition is orthogonal and therefore fully distinguishable from the initial state. If we can further ensure that, by resorting to means such as those described in the context of temperature and pressure, variations of the phase with the location and direction relative to the neutrino source as well as the use of different materials, *only* neutrinos have been scattered during this duration, then an orthogonal spin state detection at $\sim 10^5$ s corresponds to a single neutrino detection (a click), as we are ensuring that nothing else causes a change in the phase and the chance of more than one neutrino having interacted with the gram scale detector is vanishingly small.

Using an array of 10^4 such gram scale detectors, we should be able to ensure that one neutrino is detected every 10 s.

Note also that one can shorten both the duration of the experiment to τ/n and the mass required to m/n while keeping the detectability of the phase effect at the same level by using n^4 crystals. Each such crystal will get n times the velocity kick of a single crystal of mass m for the same t_{acc} or t_{kick} (we assume $\tau/n \gg t_{\text{acc}}, t_{\text{kick}}$). Thus, the timescale of generation of a superposition of given size Δx will become shortened to τ/n . Note that the phase accrued by *each* crystal in this shorter time will decrease by a factor of n^2 , i.e., ϕ becomes ϕ/n^2 as both the time and the mass to which the phase is directly proportional, decrease by n . Because of shot noise scaling n^4 interferometers can measure a phase of ϕ/n^2 with the same accuracy by measuring the spins of each interferometer. However, if one *only* reduced either the mass or the time of the interferometer by a factor of n , then we would need n^2 detectors to achieve the same scaling. For example, if we were to split the system to milligram detectors, each with superposition size of 10^{-14} m (note that this superposition size is much smaller than that required for all other suggested applications and much smaller than those achieved for atoms and macromolecules), then we would need a million such detectors. Also note that recently large masses have been prepared in nearly the ground quantum state by feedback cooling [22]—so, by similar technology, one should also be able to prepare gram scale masses in pure quantum states, which can be a starting point of creating superpositions.

VI. CHALLENGES

We have discussed the conditions needed to meet one of the principal challenges, namely, environment-induced decoherence, in the previous section while discussing the generation of the superposition. However, we discuss below how some of the other requirements may be met.

A. Satisfying the requirements of the crystal wave packet

Note that the initial spread σ_c of each of the superposed Gaussian wave packets of the crystal are required to satisfy a couple of conditions to meet some of the simplifying approximations of our calculations. Note that the position degree of freedom of all the nuclei (being part of a solid) are, to a good approximation (at least at the temperatures we consider) rigidly tied to the center of mass of the crystal and thereby has the same position spread σ_c as that of the whole crystal. As stated in Sec. II, we require $\sigma_c \lesssim 1/q_x$, relating to the momentum transferred, which in this case boils down to ensuring $\sigma_c \lesssim \Delta x \sim 10^{-14}$ m. However, we also require the initial maximum momenta of the crystal $k_i \sim 1/\sigma_c \lesssim m_{\text{nucl}} \sim 10^{-17}$ m, which stems from the assumption of the heavy nucleus being effectively at rest. Thus, there is a window. An initial diamagnetic trap of 10^5 Hz in the x direction will thus do the job, with the ground state spread of the center of mass of the crystal in such a trap being $\sim 10^{-16}$ m.

B. Coherence length of the neutrino

The consideration of processes involving neutrinos brings about several unknowns, one of which is the particle's

coherence length. In Ref. [55] the authors opted for a wave-packet treatment of the neutrino and estimated that an energy uncertainty of $\sigma_{\text{wp}} = \frac{\sigma_v}{E(p_v)} \sim 0.01$ or larger would influence decoherence and dispersion effects and thereby reduce the detector efficiency of reactor antineutrino oscillation experiments. We take this value as a reference to estimate whether a scattering event could resolve the position of our nucleus and hence spoil the superposition. Considering $\sigma_x \sigma_v \sim \frac{\hbar}{2}$, we obtain an uncertainty $\sigma_x \sim 3 \times 10^{-12}$ m for a neutrino with energy $E_v \sim 10$ MeV. This means that a neutrino with $\sigma_{\text{wp}} \sim 0.01$ would indeed be able to resolve the position of any quantum object in a superposition larger than σ_x . Seeing as the matter of the actual wave-packet shape and coherence length of the neutrino is not solved, our proposed experiment may also be able to serve as a means of testing the validity of plane wave approximations of the neutrino wave packet. Depending on the true wave-packet shape of the neutrino, we expect to observe either a coherent phase gain or a decoherence effect.

C. Lattice defects

The authors of Ref. [56] considered the structural damage effects of dark matter and neutrino scattering on dense materials with defect centers, such as nitrogen vacancy centers in diamond. In general, the deposited kinetic energies will exceed typical lattice binding energies of $\mathcal{O}(10)$ eV. Hence, we anticipate the scattering of a neutrino to lead to the formation of such damage clusters, though they can be expected to be significantly smaller in size. Based on the analysis in Ref. [56], we estimate that a nucleus recoiling with an average kinetic energy of 3 keV could generate $\mathcal{O}(10)$ lattice defects or interstitial sites. We require that these sites are created in such a manner that we cannot tell from which part of the superposition the neutrino has scattered. Here this requirement is naturally fulfilled as the size of the superposition is much smaller than the interatomic spacing in the lattice.

D. Distribution of momentum

It is the center of mass of the whole crystal which is coupled to the embedded spin used for the superposition creation/recombination and the phase read-out. However, the neutrino is initially going to impart its energy to one of the nuclei in the whole crystal. At this stage, the energy imparted is localized to this nucleus, but the center of mass already has the imparted momentum; however, the crystal cannot be considered as all rigidly connected nuclei moving together, which is required for the embedded spin to sense the transferred momentum. A local phonon is excited in the crystal at the site of the scattering neutrino. However, phonon relaxation times in crystals are generally ~ 1 – 100 ns [57], after which the energy would have been transferred to the center of mass of the whole crystal.

VII. DISCUSSION

We have described the detection of neutrinos from the relative phase they impart between the components of a quantum superposition of two spatially localized states of the center of mass of a crystal. As naturally there is a distribution of

momentum after the scattering, this process also causes a decoherence in addition to imparting a change in the relative phase. We thus formulated a master equation technique to evolve the full density matrix of the COM of a crystal under the scenario of the scattering of a relativistic particle from it. Solving that, we found that the optimal detection requires a ~ 1 g mass placed in a quantum superposition of states separated by a distance $\Delta x \sim 10^{-14}$ m. For completeness, we have also suggested a schematic and parameter domain by adopting which such superpositions could be achieved and maintained for the long duration of our experiment, although much more analysis will be required for realistic scenarios.

It is worth clarifying the role of the various ingredients of our method proposed herewith. The superposition serves as a means to detect the momentum recoil k of the crystal in terms of the relative phase $k\Delta x$. Of course, that will happen for a crystal of any mass, including individual atoms in a superposition of states separated by Δx . However, in that case the cross section is very small. For a crystal of N_{Atoms} , the cross section is amplified N_{Atoms} times. While an uncorrelated collection of N_{Atoms} in the same superposition state will have the same cross section, the neutrino will only scatter from one of those atoms, and one has to measure each atom after appropriate basis rotations to measure whether one of them obtained a phase. In the case of a crystal with a single embedded spin, the phase gained by the neutrino hitting any one of the nuclei is mapped on to the relative phase between the COM states of the whole crystal. This is because of the very strong correlations between the positions of the atoms the N_{Atoms} , since they are all either clustered around the state $|\bar{x}_0\rangle$ or the state $|\bar{x}_1\rangle$. The positions of all the atoms are entangled when the center of mass is placed in the superposition $|\bar{x}_0\rangle + |\bar{x}_1\rangle$. Moreover, due to the very mechanism of our interferometry, the embedded spin or other ancillary system is also entangled with the center of mass during the interferometry, so that at the end, the phase can be estimated exclusively by measuring this single spin. The reason that we have used a regime in which the scattering from each nucleus is coherent is because it enhances the cross section by N^2 times (N being the number of neutrons in a nucleus), which makes our times-scales about 10^4 times less than what it would have been otherwise.

It is important to clarify that going to either higher or lower energy neutrinos is not a trivial problem. For higher energies, it is true that the cross section increases as $\propto E^2$, where E is the energy of the incident neutrinos. However, the momentum transferred may be too high and knock a nucleus completely out of the crystal so that the momentum is not imparted to the rest of the crystal. Moreover, $k\Delta x \sim 1$ implies that much smaller superpositions Δx will have to be used, which implies a great difficulty in satisfying our simplification assumptions $1/m_{\text{nucl}} \ll \sigma_c \ll \Delta x \sim 1/k$ and the calculations will be needed to be performed in much more generality. For lower energies, cross section can both decrease due to the $\propto E^2$ effect or increase due to scope of scattering coherently from all atoms of the crystal. However, producing a larger $\Delta x \sim 1/k$ superposition becomes much more difficult, especially for the masses as large as the ones that are needed here.

Our technique presented in this work should be adaptable to any relativistic particles scattering off a quantum superposition with appropriate modifications. Moreover, neutrinos will form a background to any other signals one may want to detect. The calculations here show that even a substantially large mass in a quantum superposition of distinct spatial states can remain coherent for a very long time close to a source of neutrinos so that there is an ample window for the detection of other signals.

ACKNOWLEDGMENTS

E.K. acknowledges support from the Engineering and Physical Sciences Research Council (Grant No. EP/L015242/1). M.T. and S.B. acknowledge EPSRC Grant No. EP/N031105/1, S.B. the EPSRC Grant No. EP/S000267/1, and M.T. funding by the Leverhulme Trust (Grant No. RPG-2020-197). F.F.D. acknowledges support from a UK STFC consolidated grant (Reference No. ST/P00072X/1). R.S. acknowledges support from the Science and Technology Facilities Council (Grant No. ST/T006439/1).

-
- [1] F. Reines and C. L. Cowan, Jr., The Neutrino, *Nature* **178**, 446 (1956).
- [2] Y. Fukuda, T. Hayakawa, E. Ichihara, K. Inoue, K. Ishihara, H. Ishino, Y. Itow, T. Kajita, J. Kameda, S. Kasuga *et al.*, Evidence for Oscillation of Atmospheric Neutrinos, *Phys. Rev. Lett.* **81**, 1562 (1998).
- [3] The KATRIN Collaboration, M. Aker, A. Beglarian, J. Behrens, A. Berlev, U. Besserer, B. Bieringer, F. Block, S. Bobien, M. Böttcher, B. Borschein *et al.*, Direct neutrino-mass measurement with sub-electronvolt sensitivity, *Nat. Phys.* **18**, 160 (2022).
- [4] S. Bose, K. Jacobs, and P. L. Knight, Scheme to probe the decoherence of a macroscopic object, *Phys. Rev. A* **59**, 3204 (1999).
- [5] A. D. Armour, M. P. Blencowe, and K. C. Schwab, Entanglement and Decoherence of a Micromechanical Resonator Via Coupling to a Cooper-Pair Box, *Phys. Rev. Lett.* **88**, 148301 (2002).
- [6] W. Marshall, C. Simon, R. Penrose, and D. Bouwmeester, Toward Quantum Superpositions of a Mirror, *Phys. Rev. Lett.* **91**, 130401 (2003).
- [7] O. Romero-Isart, Quantum superposition of massive objects and collapse models, *Phys. Rev. A* **84**, 052121 (2011).
- [8] O. Romero-Isart, A. C. Pflanzer, F. Blaser, R. Kaltenbaeck, N. Kiesel, M. Aspelmeyer, and J. I. Cirac, Large Quantum Superpositions and Interference of Massive Nanometer-Sized Objects, *Phys. Rev. Lett.* **107**, 020405 (2011).

- [9] J. Bateman, S. Nimmrichter, K. Hornberger, and H. Ulbricht, Near-field interferometry of a free-falling nanoparticle from a point-like source, *Nat. Commun.* **5**, 4788 (2014).
- [10] M. Scala, M. S. Kim, G. W. Morley, P. F. Barker, and S. Bose, Matter-Wave Interferometry of a Levitated Thermal Nano-Oscillator Induced and Probed by a Spin, *Phys. Rev. Lett.* **111**, 180403 (2013).
- [11] Z. Q. Yin, T. Li, X. Zhang, and L. M. Duan, Large quantum superpositions of a levitated nanodiamond through spin-optomechanical coupling, *Phys. Rev. A* **88**, 033614 (2013).
- [12] C. Wan, M. Scala, G. W. Morley, A. A. Rahman, H. Ulbricht, J. Bateman, P. F. Barker, S. Bose, and M. S. Kim, Free Nano-Object Ramsey Interferometry for Large Quantum Superpositions, *Phys. Rev. Lett.* **117**, 143003 (2016).
- [13] J. S. Pedernales, G. W. Morley, and M. B. Plenio, Motional Dynamical Decoupling for Interferometry with Macroscopic Particles, *Phys. Rev. Lett.* **125**, 023602 (2020).
- [14] Y. Margalit, O. Dobkowski, Z. Zhou, O. Amit, Y. Japha, S. Moukouri, D. Rohrlach, A. Mazumdar, S. Bose, C. Henkel *et al.*, Realization of a complete stern-gerlach interferometer: Toward a test of quantum gravity, *Sci. Adv.* **7**, eabg2879 (2021).
- [15] B. D. Wood, S. Bose, and G. W. Morley, Spin dynamical decoupling for generating macroscopic superpositions of a free-falling nanodiamond, *Phys. Rev. A* **105**, 012824 (2022).
- [16] R. J. Marshman, A. Mazumdar, R. Folman, and S. Bose, Large splitting massive Schrödinger kittens, *Phys. Rev. Res.* **4**, 023087 (2022).
- [17] Y. Y. Fein, P. Geyer, P. Zwick, F. Kiałka, S. Pedalino, M. Mayor, S. Gerlich, and M. Arndt, Quantum superposition of molecules beyond 25 kDa, *Nat. Phys.* **15**, 1242 (2019).
- [18] L. Magrini, P. Rosenzweig, C. Bach, A. Deutschmann-Olek, S. G. Hofer, S. Hong, N. Kiesel, A. Kugi, and M. Aspelmeyer, Real-time optimal quantum control of mechanical motion at room temperature, *Nature* **595**, 373 (2021).
- [19] U. Delić, M. Reisenbauer, K. Dare, D. Grass, V. Vuletić, N. Kiesel, and M. Aspelmeyer, Cooling of a levitated nanoparticle to the motional quantum ground state, *Science* **367**, 892 (2020).
- [20] F. Tebbenjohanns, M. Frimmer, V. Jain, D. Windey, and L. Novotny, Motional Sideband Asymmetry of a Nanoparticle Optically Levitated in Free Space, *Phys. Rev. Lett.* **124**, 013603 (2020).
- [21] F. Tebbenjohanns, M. L. Mattana, M. Rossi, M. Frimmer, and L. Novotny, Quantum control of a nanoparticle optically levitated in cryogenic free space, *Nature* **595**, 378 (2021).
- [22] C. Whittle, E. D. Hall, S. Dwyer, N. Mavalvala, V. Sudhir, R. Abbott, A. Ananyeva, C. Austin, L. Barsotti, J. Betzwieser *et al.*, Approaching the motional ground state of a 10-kg object, *Science* **372**, 1333 (2021).
- [23] M. Rademacher, J. Millen, and Y. L. Li, Quantum sensing with nanoparticles for gravimetry: When bigger is better, *Adv. Opt. Technol.* **9**, 227 (2020).
- [24] R. J. Marshman, A. Mazumdar, G. W. Morley, P. F. Barker, S. Hoekstra, and S. Bose, Mesoscopic interference for metric and curvature and gravitational wave detection, *New J. Phys.* **22**, 083012 (2020).
- [25] S. Bose, A. Mazumdar, G. W. Morley, H. Ulbricht, M. Toroš, M. Paternostro, A. A. Geraci, P. F. Barker, M. S. Kim, and G. Milburn, Spin Entanglement Witness for Quantum Gravity, *Phys. Rev. Lett.* **119**, 240401 (2017).
- [26] C. Marletto and V. Vedral, Gravitationally Induced Entanglement between Two Massive Particles is Sufficient Evidence of Quantum Effects in Gravity, *Phys. Rev. Lett.* **119**, 240402 (2017).
- [27] R. J. Marshman, A. Mazumdar, and S. Bose, Locality and entanglement in table-top testing of the quantum nature of linearized gravity, *Phys. Rev. A* **101**, 052110 (2020).
- [28] S. Bose, A. Mazumdar, M. Schut, and M. Toroš, Mechanism for the quantum natured gravitons to entangle masses, *Phys. Rev. D* **105**, 106028 (2022).
- [29] P. F. Barker, S. Bose, R. J. Marshman, and A. Mazumdar, Entanglement based tomography to probe new macroscopic forces, *Phys. Rev. D* **106**, L041901 (2022).
- [30] S. Bose, A. Mazumdar, M. Schut, and M. Toroš, Entanglement witness for the weak equivalence principle, *Entropy* **25**, 448 (2022).
- [31] C. J. Riedel, Direct detection of classically undetectable dark matter through quantum decoherence, *Phys. Rev. D* **88**, 116005 (2013).
- [32] C. J. Riedel, Decoherence from classically undetectable sources: Standard quantum limit for diffusion, *Phys. Rev. A* **92**, 010101(R) (2015).
- [33] C. J. Riedel and I. Yavin, Decoherence as a way to measure extremely soft collisions with dark matter, *Phys. Rev. D* **96**, 023007 (2017).
- [34] F. Monteiro, G. Afek, D. Carney, G. Krnjaic, J. Wang, and D. C. Moore, Search for Composite Dark Matter with Optically Levitated Sensors, *Phys. Rev. Lett.* **125**, 181102 (2020).
- [35] G. Afek, D. Carney, and D. C. Moore, Coherent Scattering of Low Mass Dark Matter from Optically Trapped Sensors, *Phys. Rev. Lett.* **128**, 101301 (2022).
- [36] D. Z. Freedman, Coherent effects of a weak neutral current, *Phys. Rev. D* **9**, 1389 (1974).
- [37] D. Akimov, J. B. Albert, P. An, C. Awe, P. S. Barbeau, B. Becker, V. Belov, A. Brown, A. Bolozdynya, B. Cabrera-Palmer *et al.*, Observation of coherent elastic neutrino-nucleus scattering, *Science* **357**, 1123 (2017).
- [38] V. Domcke and M. Spinrath, Detection prospects for the cosmic neutrino background using laser interferometers, *J. Cosmol. Astropart. Phys.* **6**, 055 (2017).
- [39] R. Strauss, J. Rothe, G. Angloher, A. Bento, A. Gütlein, D. Hauff, H. Kluck, M. Mancuso, L. Oberauer, F. Petricca, F. Pröbst, J. Schieck, S. Schönert, W. Seidel, and L. Stodolsky, The ν -cleus experiment: A gram-scale fiducial-volume cryogenic detector for the first detection of coherent neutrino-nucleus scattering, *Eur. Phys. J. C* **77**, 506 (2017).
- [40] N. Bar-Gill, L. M. Pham, A. Jarmola, D. Budker, and R. L. Walsworth, Solid-state electronic spin coherence time approaching one second, *Nat. Commun.* **4**, 1743 (2013).
- [41] M. Niethammer, M. Widmann, T. Rendler, N. Morioka, Y.-C. Chen, R. Stöhr, J. U. Hassan, S. Onoda, T. Ohshima, S.-Y. Lee *et al.*, Coherent electrical readout of defect spins in silicon carbide by photo-ionization at ambient conditions, *Nat. Commun.* **10**, 5569 (2019).
- [42] A. M. Jakob, S. G. Robson, V. Schmitt, V. Mourik, M. Posselt, D. Spemann, B. C. Johnson, H. R. Fergau, E. Mayes, J. C. McCallum *et al.*, Deterministic shallow dopant implantation in silicon with detection confidence upper-bound to

- 99.85% by ion–solid interactions, *Adv. Mater.* **34**, 2103235 (2022).
- [43] M. Keil, S. Machluf, Y. Margalit, Z. Zhou, O. Amit, O. Dobkowsky, Y. Japha, S. Moukouri, D. Rohrich, Z. Binstock *et al.*, Stern-Gerlach Interferometry with the Atom Chip, in *Molecular Beams in Physics and Chemistry*, edited by B. Friedrich and H. Schmidt-Böcking (Springer, Cham, 2021), pp. 263–301.
- [44] M. Lindner, W. Rodejohann, and X.-J. Xu, Coherent neutrino-nucleus scattering and new neutrino interactions, *J. High Energy Phys.* **03** (2017) 097.
- [45] K. Scholberg, Coherent elastic neutrino-nucleus scattering, *J. Phys.: Conf. Ser.* **606**, 012010 (2015).
- [46] G. S. Agarwal, *Quantum Optics* (Cambridge University Press, Cambridge, UK, 2012).
- [47] M. D. Schwartz, *Quantum Field Theory and the Standard Model* (Cambridge University Press, New York, NY, 2014).
- [48] M. R. Gallis and G. N. Fleming, Environmental and spontaneous localization, *Phys. Rev. A* **42**, 38 (1990).
- [49] D. Lunney, J. M. Pearson, and C. Thibault, Recent trends in the determination of nuclear masses, *Rev. Mod. Phys.* **75**, 1021 (2003).
- [50] A. C. Hayes and P. Vogel, Reactor neutrino spectra, *Annu. Rev. Nucl. Part. Sci.* **66**, 219 (2016).
- [51] Y. Kim, Detection of antineutrinos for reactor monitoring, *Nucl. Eng. Technol.* **48**, 285 (2016).
- [52] M. A. Nielsen and I. Chuang, *Quantum Computation and Quantum Information* (Cambridge University Press, Cambridge, 2010).
- [53] M. Zhong, M. P. Hedges, R. L. Ahlefeldt, J. G. Bartholomew, S. E. Beavan, S. M. Wittig, J. J. Longdell, and M. J. Sellars, Optically addressable nuclear spins in a solid with a six-hour coherence time, *Nature* **517**, 177 (2015).
- [54] D. E. Chang, C. Regal, S. Papp, D. Wilson, J. Ye, O. Painter, H. J. Kimble, and P. Zoller, Cavity opto-mechanics using an optically levitated nanosphere, *Proc. Natl. Acad. Sci. USA* **107**, 1005 (2010).
- [55] Y.-L. Chan, M.-C. Chu, K. M. Tsui, C. F. Wong, and J. Xu, Wave-packet treatment of reactor neutrino oscillation experiments and its implications on determining the neutrino mass hierarchy, *Eur. Phys. J. C* **76**, 310 (2016).
- [56] S. Rajendran, N. Zobrist, A. O. Sushkov, R. Walsworth, and M. Lukin, A method for directional detection of dark matter using spectroscopy of crystal defects, *Phys. Rev. D* **96**, 035009 (2017).
- [57] H. Zhao and J. B. Freund, Full-spectrum phonon relaxation times in crystalline Si from molecular dynamics simulations, *J. Appl. Phys.* **104**, 033514 (2008).